



Pacific Northwest
NATIONAL LABORATORY

*Proudly Operated by **Battelle** Since 1965*

Optimizing Lidar Wind Measurements from the DOE WindSentinel Buoys

June 2016

RK Newsom

DISCLAIMER

This report was prepared as an account of work sponsored by an agency of the United States Government. Neither the United States Government nor any agency thereof, nor Battelle Memorial Institute, nor any of their employees, makes **any warranty, express or implied, or assumes any legal liability or responsibility for the accuracy, completeness, or usefulness of any information, apparatus, product, or process disclosed, or represents that its use would not infringe privately owned rights.** Reference herein to any specific commercial product, process, or service by trade name, trademark, manufacturer, or otherwise does not necessarily constitute or imply its endorsement, recommendation, or favoring by the United States Government or any agency thereof, or Battelle Memorial Institute. The views and opinions of authors expressed herein do not necessarily state or reflect those of the United States Government or any agency thereof.

PACIFIC NORTHWEST NATIONAL LABORATORY
operated by
BATTELLE
for the
UNITED STATES DEPARTMENT OF ENERGY
under Contract DE-AC05-76RL01830

Printed in the United States of America

Available to DOE and DOE contractors from the
Office of Scientific and Technical Information,
P.O. Box 62, Oak Ridge, TN 37831-0062;
ph: (865) 576-8401
fax: (865) 576-5728
email: reports@adonis.osti.gov

Available to the public from the National Technical Information Service
5301 Shawnee Rd., Alexandria, VA 22312
ph: (800) 553-NTIS (6847)
email: orders@ntis.gov <<http://www.ntis.gov/about/form.aspx>>
Online ordering: <http://www.ntis.gov>



This document was printed on recycled paper.

(8/2010)

Optimizing Lidar Wind Measurements from the DOE WindSentinel Buoys

RK Newsom

June 2016

Prepared for
the U.S. Department of Energy
under Contract DE-AC05-76RL01830

Pacific Northwest National Laboratory
Richland, Washington 99352

Abstract

During the period from December 2014 to June 2016, a U.S. Department of Energy (DOE) WindSentinel buoy was deployed off the Virginia coast in support of an offshore wind energy demonstration project funded by the DOE Office of Energy Efficiency and Renewable Energy (EERE). The buoy was equipped with a Vindicator III Doppler lidar, manufactured by Optical Air Data Systems (OADS), and a host of other meteorological and oceanographic instruments. Initial analyses of the 10-minute average wind speeds from the lidar shows a consistent negative shear in the upper range gates of the lidar, resulting in an apparent low-level jet (LLJ) feature with a wind speed maximum near the 90 m level.

The apparent maximum in the wind speed profile is believe to be the result of slow biases in the upper range gates due to weak backscatter signals. In this study, we attempt to address this issue by first examining the OADS wind retrieval algorithm used to generate the 1Hz Vindicator data, from which 10-minute average wind speed and direction profiles are computed. We find that the OADS approach is fundamentally sound, but the quality of the 10-minute averages could be improved by applying a higher signal strength threshold to the 1Hz data.

We show that the overall effect of the signal strength threshold is to decrease the magnitude of the shear, both above and below the apparent maxima in the wind speed profile. The effect is most pronounced in the highest range gates where the return signal strength is generally weakest. An undesired side effect is a substantial reduction in the data recovery rate. For a signal strength threshold of 60, the annually averaged data recovery rate was about 75% for the best case (range gate 3), and about 15 to 20% for the worst case (range gate 6). Data recovery rates are higher during the warm season and during daytime periods.

Acronyms and Abbreviations

AGL	above ground level
AHRS	Attitude and Heading Reference System
ARM	Atmospheric Radiation Measurement Climate Research Facility
BAO	Boulder Atmospheric Observatory
DOE	U.S. Department of Energy
EERE	DOE Office of Energy Efficiency and Renewable Energy
Hz	hertz
kHz	kilohertz
LLU	low level jet
OADS	Optical Air Data Systems
PNNL	Pacific Northwest National Laboratory
SNR	signal-to-noise ration
XPIA	eXperimental Planetary boundary-layer Instrument Assessment
UTC	Coordinated Universal Time

Contents

Abstract	iii
Acronyms and Abbreviations	v
1.0 Introduction	1
2.0 Vindicator III Lidar	4
3.0 OADS Wind Retrieval and Attitude Correction	6
4.0 PNNL Wind Retrieval and Results	10
5.0 Summary	16
6.0 References	17
Appendix A Vindicator versus Tower Comparison during XPIA	A.1
Appendix B Data File Description and Format for the 1 Hz OADS Vindicator III Data	B.4

Figures

1. Data flow for the WindSentinel lidar data	2
2. Median wind speed (red) and median signal-strength (blue) from a) the Vindicator III on Virginia buoy for the period from 13 December, 2014 to 8 March, 2016, and b) from the Vindicator III (S/N 3013) during the XPIA field campaign from 8 April to 29 May, 2015.	3
3. a) The Vindicator III lidar, and b) the buoy with the laser beams and range gate centers indicated. ...	5
4. Coordinate system and beam geometry for the Vindicator III Doppler lidar. a) top view, and b) side view.	6
5. Time series of roll, pitch, and yaw from the Vindicator III AHRS unit on the Virginia buoy between 18:00 to 19:00 UTC on 10 May, 2015.	9
6. Representative time series of 1 Hz a) wind speed and b) wind direction of the smoothed OADS (red) and unsmoothed (blue) retrievals.	10
7. Doppler frequency shift estimation in the weak signal regime.	11
8. Mean wind speed shear between third and fifth gates (blue) and third and sixth range gates (red) as a function of signal strength threshold, S_T	12
9. Distributions of the surface wind speed for $S_6 > 100$ (red) and $S_6 < 100$ (blue).	13
10. a) Diurnal and b) seasonal data recovery (solid) and signal strength (dashed) for $S_T=60$	14
11. Mean daytime wind speed (a) and shear (b) profiles for the period from 1 June through 30 September, 2015 using $S_T=0$ (blue) and $S_T=60$ (red).	15
12. 10-minute-averaged lidar measurement heights (red) for the month of June 2015.	16

Tables

1. Vindicator III optical unit specifications.	4
2. Mean measurement heights (third column) and corresponding standard deviations (fourth column) for the period from 13 December, 2014 to 8 March, 2016.	16

1.0 Introduction

Pacific Northwest National Laboratory (PNNL) manages the deployment and operation of two WindSentinel buoys from AXYS Technologies for the U.S. Department of Energy (DOE). These buoys provide data for a variety of research and development activities aimed at accelerating the development of offshore wind plants in U.S. waters. Each buoy is equipped with a Vindicator III lidar manufactured by Optical Air Data Systems (OADS). The Vindicator is a coherent Doppler lidar that provides measurements of wind speed and direction at six levels up to a maximum height of approximately 180 m above the ocean surface. This enables the WindSentinel to measure winds over the full height of a typical offshore wind turbine. In addition to the lidar, each buoy is also equipped with a suite of meteorological and oceanographic sensors. These sensors provide measurements of surface winds, relative humidity, temperature, wave characteristics, and other variables.

In December 2014 one of the DOE WindSentinel buoys was deployed approximately 42 km off the Virginia coast. Since that time, the buoy has operated nearly continuously and collected a wealth of information. Initial analyses of the 10-minute average wind speeds from the lidar shows a consistent negative shear in the upper range gates of the lidar, resulting in an apparent low-level jet (LLJ) feature with a wind speed maximum near the 90 m level. These results are similar to those obtained during a recent land-based field campaign at the Boulder Atmospheric Observatory (BAO) in April and May of 2015 (Lundquist et al. 2016). During that field campaign, 10-minute average measurements from two Vindicator lidars were compared to sonic anemometer measurements on the 300-m BAO tower. The lidar-derived winds showed a significant slow bias in the highest lidar range gates as compared to the tower.

The goal of this study is to identify the cause of the observed wind speed bias, and to evaluate methods of processing the raw lidar data that could potentially reduce these biases. During the BAO field study, we found that biases in the 10-minute Vindicator winds could be reduced by reprocessing the raw lidar data using more aggressive rejection of low signal-to-noise-ratio (SNR) measurements. The approach in this study is to first reproduce the OADS 1Hz wind measurements from the raw radial velocity and platform attitude information, and then make appropriate modifications to the OADS data-processing scheme in an effort to reduce the observed wind speed biases.

Figure 1 shows a simplified high-level data flow diagram for the lidar wind data product. The Vindicator III outputs 1 Hz data files containing measurements of radial velocity, backscatter signal strength, roll, pitch, yaw, latitude, longitude, wind speed, wind direction, vertical velocity, and various ancillary fields describing the health of the system (a complete listing of the format is provided in Appendix B). The 1 Hz wind speed, wind direction, and vertical velocity data are then ingested by the AXYS Watchman 500 data system and averaged down to 10 minutes. The 10-minute averages output by the Watchman 500 are broadcast to shore in near-real time using either satellite or cellular communications. Due to bandwidth limitations, the original 1 Hz data are not broadcast but instead stored locally on a compact flashcard. Currently, the only way to retrieve the 1 Hz data is to physically board the buoy and pull the flashcard.

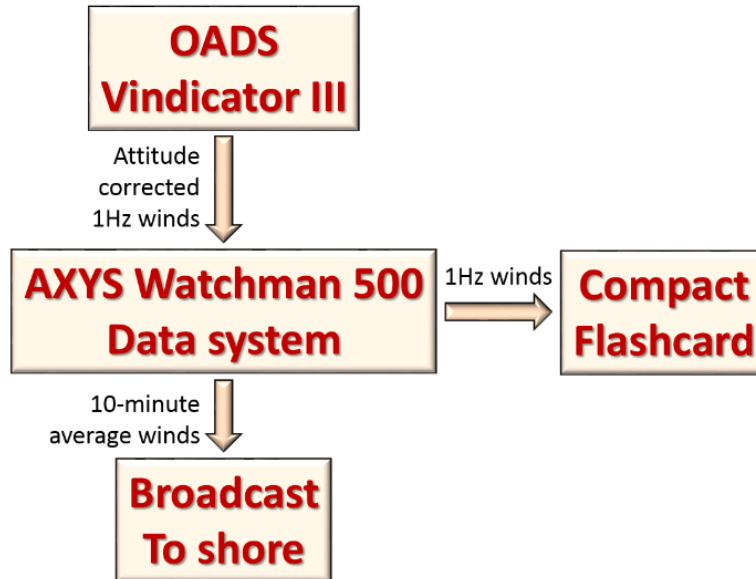


Figure 1. Data flow for the WindSentinel lidar data.

As of June 2016, there have been two maintenance visits to the Virginia buoy. The first visit occurred on 28 July, 2015 and the second visit occurred on 8 March, 2016. During both visits, the compact flashcards were retrieved and replaced with new cards. As a result, PNNL currently possess raw 1Hz lidar data from the Virginia deployment spanning the period from about 12 December, 2014 to 8 March, 2016. PNNL’s modified data-processing method has been applied to this entire period.

Coherent Doppler Lidars, such as the Vindicator, produce range-resolved estimates of radial velocity and some measure of the coherent signal strength. Different manufacturers have different methods of quantifying the return signal strength. A common metric that is used is the so-called wide-band SNR. This is the ratio of the total signal energy to the total noise energy integrated over the receiver passband (Pearson et al. 2009). The wide-band SNR is typically much less than one for diffuse aerosol targets. Alternatively, the narrow-band SNR can be computed from the ratio of the peak power to the average noise power in the Doppler spectrum. This method produces values that are greater than unity, as is the case with the signal strength parameter reported in the 1Hz data files.

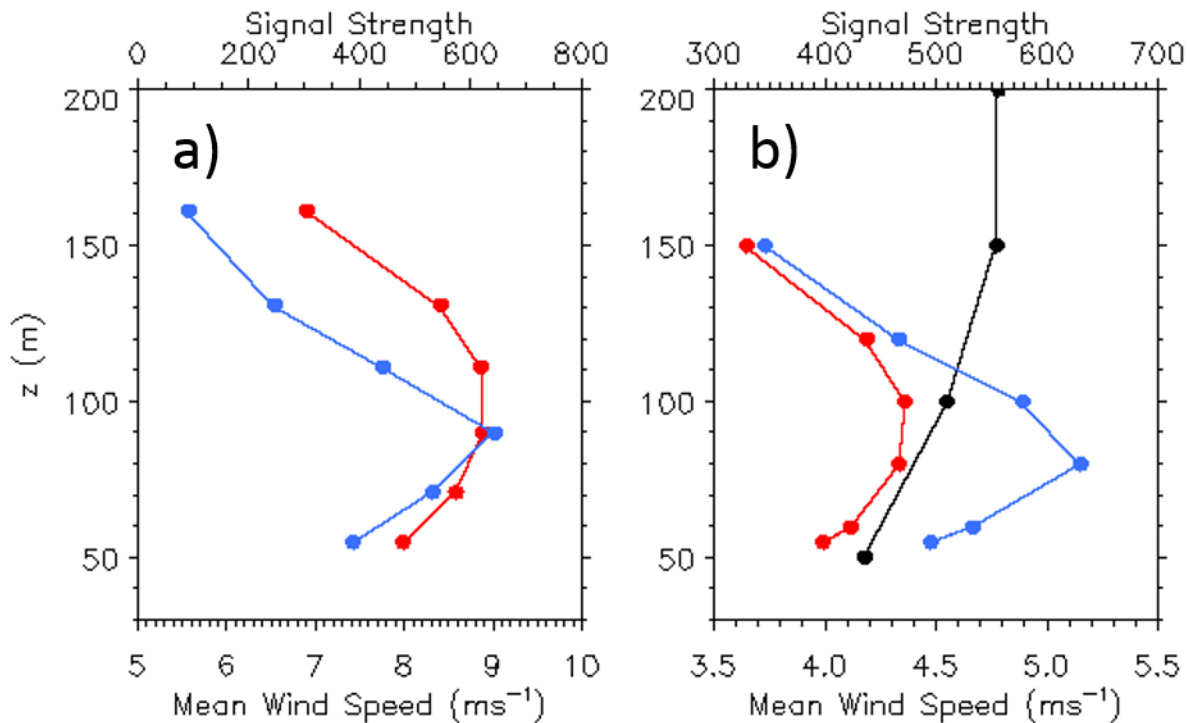


Figure 2. Median wind speed (red) and median signal-strength (blue) from a) the Vindicator III on Virginia buoy for the period from 13 December, 2014 to 8 March, 2016, and b) from the Vindicator III (S/N 3013) during the XPIA field campaign from 8 April to 29 May, 2015. The black curve in panel b) is the median wind speed profile from the sonic anemometers on the 300 m BAO tower.

Figure 2a shows median wind speed and signal strength profiles from the Vindicator III lidar during the Virginia deployment from 13 December, 2014 to 8 March, 2016. For comparison, Fig 2b shows the median wind speed and signal strength profiles from a different Vindicator III lidar (S/N 3013) during the XPIA field campaign. Also shown in Fig 2b is the median wind speed profile from the sonic anemometers on the 300 m BAO tower. The wind speed profiles were computed from the 10-minute data product generated by the Watchman 500, whereas the signal strength profiles were computed from the 1Hz lidar data. In both cases, the signal strength profiles exhibit prominent maxima near the 80-to-90 m range gates, and the wind speed profiles exhibit maxima at or slightly above these levels. Comparison with the BAO profile in Figure 2b clearly shows that the Vindicator III is biased low in the uppermost and lowermost range gates. The bias is particularly large in the highest range gates where the signal strength is weakest. We also note that the wind speed profiles in Figure 2 are similar in shape to those obtained during the initial performance evaluation of the Virginia buoy in the Strait of Juan de Fuca in October 2014 (Newsom et al. 2015). For the current study, we are focused on reducing the apparent biases in the 10-minute data product from the Vindicator III during the deployment off the Virginia coast. To this end, we examine the OADS wind retrieval algorithm and investigate the effectiveness of filtering the data based on the signal strength. For reference, the results from the XPIA field campaign are also briefly summarized in Appendix A.

This report is organized as follows: Section 2 gives a brief description of the Vindicator III lidar; Section 3 describes the current OADS wind retrieval and data processing method; and Section 4 describes the

modifications to the OADS processing method and presents results that quantify the improvement in data quality as a result of these modifications. Lastly, the results of this study are summarized in Section 5.

2.0 Vindicator III Lidar

The OADS Vindicator III lidar is a compact coherent Doppler lidar that operates by transmitting three simultaneous pulsed laser beams into the atmosphere. The laser light scatters off particulates as the pulses travel through the atmosphere. A small fraction of that scattered light (i.e., backscatter) is collected by the lidar receiver and combined with a reference laser beam (i.e., the local oscillator) and then detected. The superposition of the backscatter with the reference results in a sinusoidal modulation the frequency of which is equal to the difference between the backscatter and the reference. The combined signal is gated in time so that each gate or bin represents a measurement at a particular range from the lidar. The gated signals are then spectrally analyzed to determine the Doppler shift (i.e., the modulation frequency) within each range gate. These Doppler shifts are then converted to radial velocity using $u_r = f_d \lambda / 2$, where f_d is the Doppler shift frequency, λ is the laser wavelength, and u_r is the radial velocity.

Table 1. Vindicator III optical unit specifications.

Operating Wavelength	1550 nm
Wind speed range	0 to 90 ms ⁻¹
Sensing Range	30 to 180 m
Maximum range gates	6
Range gate Length	40 m
Pulse repetition rate	1-10 kHz
Laser Eye Safety	Class 1M
Dimensions	46 cm diameter
Weight	43 kg
Max power consumption	70 W

Table 1 lists the relevant performance specifications of the Vindicator III, and Figure 3 shows the lidar hardware and its location on the WindSentinel buoy. The Vindicator III uses a Class 1M eye-safe laser transmitter that operates at a wavelength of 1.5 microns and a pulse repetition frequency of between 1 and 10 kHz. The optimum sensing range is between 30 and 180 m, and there are six user configurable range gates. The gate sizes are fixed at 40 m, but the locations of the centers of these gates can be set by the user anywhere within the sensing range. For this deployment, the gate centers were placed at 55, 70, 90, 110, 130 and 160 m, as shown in Fig 3. The Vindicator III also includes an internal Attitude and Heading Reference System (AHRS) unit and an externally mounted window-cleaning system. The AHRS provides the attitude angles needed to compute the wind velocity vector in the Earth-fixed coordinate system. The window-cleaning system consists of a compressed air blower and washer fluid dispenser that keeps the laser apertures clear.

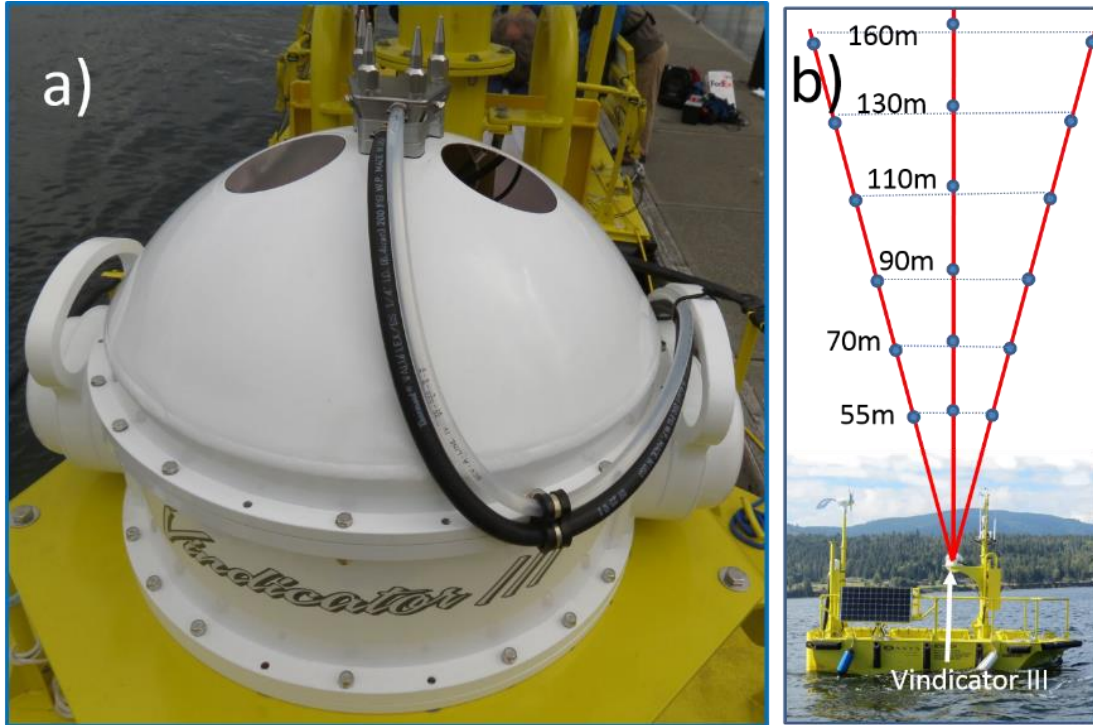


Figure 3. a) The Vindicator III lidar, and b) the buoy with the laser beams and range gate centers indicated. Specific range gate center locations shown in panel b correspond to the configuration used during the Virginia deployment.

Figure 4 shows the body coordinate system and beam geometry for the Vindicator III. Note that the laser beams do not exit perpendicular to the windows. Instead, the beams exit in such a way that they intersect at a common point about 25 cm above the lidar. Each beam forms an angle of 15° with respect to the x' axis. When projected into the y' - z' plane, beams 1 and 2 form angles of about $+103^\circ$ and -103° from the z' axis, respectively. Beam 3 forms an angle of 0° with respect to the z' axis when projected into the y' - z' plane.

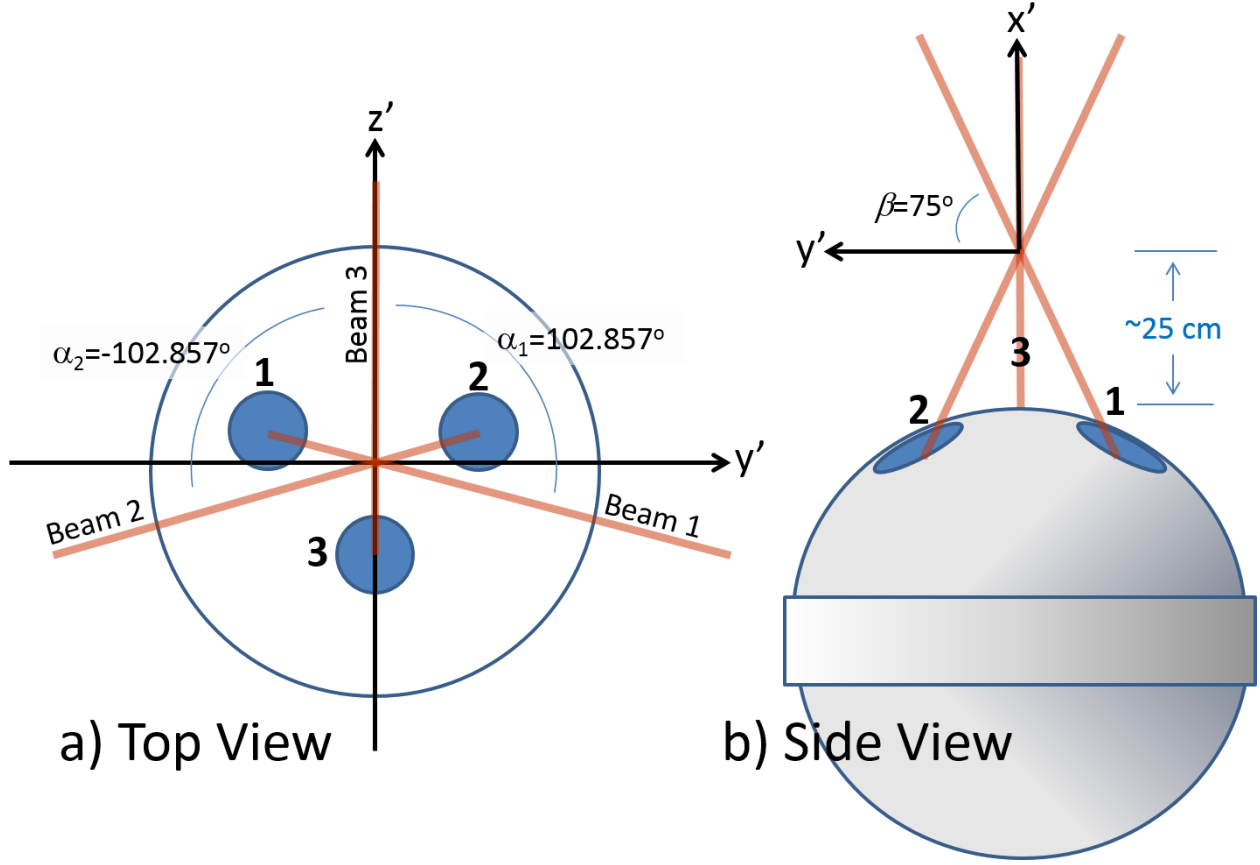


Figure 4. Coordinate system and beam geometry for the Vindicator III Doppler lidar. a) top view, and b) side view.

From the geometry shown in Fig 4, the unit vector that describes the pointing direction of the n^{th} laser beam is given by

$$\mathbf{b}_n = \mathbf{x}' \sin \beta + \mathbf{y}' \sin \alpha_n \cos \beta + \mathbf{z}' \cos \alpha_n \cos \beta \quad (1)$$

where \mathbf{x}' , \mathbf{y}' and \mathbf{z}' are unit vectors along the x' , y' and z' directions, respectively. The beam pointing directions are defined by the azimuth angles, $\alpha_1 = 102.857^\circ$, $\alpha_2 = -102.857^\circ$ and $\alpha_3 = 0^\circ$ as measured clockwise from the z' axis. The elevation angles, as measured from the y' - z' plane, are $\beta = 75^\circ$ for all three beams.

3.0 OADS Wind Retrieval and Attitude Correction

In this section we provide a step-by-step description of the OADS wind retrieval algorithm that is used to generate the 1 Hz wind speed, wind direction and vertical velocity data. Velocity vectors are retrieved from the 1 Hz radial velocity observations by assuming the velocity to be constant across the three beams for a given range gate. Initially, the retrieved vector is expressed in terms of the body coordinate system, i.e., $\mathbf{u}' = \mathbf{x}'u' + \mathbf{y}'v' + \mathbf{z}'w'$, and then transformed to an Earth-fixed frame using the roll, pitch, and yaw

information from the internal AHRS unit. This transformation constitutes the so-called motion-compensation procedure.

The observed radial velocity along the n^{th} beam at a given range gate is related to the components of the velocity vector through the following relationship

$$u_m = \mathbf{u}' \cdot \mathbf{b}_n = u' \sin \beta + v' \sin \alpha_n \cos \beta + w' \cos \alpha_n \cos \beta \quad (2)$$

Where n is the beam index such that $n=1, 2, \text{ or } 3$, and u_m is the observed radial velocity at a given range gate along the n^{th} beam. Equation (2) defines a system of three equations and three unknowns, u' , v' , and w' . The solution is obtained from

$$\begin{pmatrix} u' \\ v' \\ w' \end{pmatrix} = \begin{pmatrix} \sin \beta & \sin \alpha_1 \cos \beta & \cos \alpha_1 \cos \beta \\ \sin \beta & \sin \alpha_2 \cos \beta & \cos \alpha_2 \cos \beta \\ \sin \beta & \sin \alpha_3 \cos \beta & \cos \alpha_3 \cos \beta \end{pmatrix}^{-1} \begin{pmatrix} u_{r1} \\ u_{r2} \\ u_{r3} \end{pmatrix}. \quad (3)$$

If it is assumed that the lidar is located at the center of rotation, then the transformation from the body (primed) coordinate system to the Earth-fixed frame takes the following form:

$$\begin{pmatrix} u_{north} \\ u_{west} \\ u_{down} \end{pmatrix} = (R)(P)(Y) \begin{pmatrix} u' \\ v' \\ w' \end{pmatrix}, \quad (4)$$

where (R) , (P) , and (Y) are the rotation matrices for roll, pitch, and yaw, respectively (defined below).

The northerly, westerly, and downward velocity components are denoted u_{north} , u_{west} , and u_{down} , respectively. If we adopt the standard meteorological coordinate system in which u is the easterly component, v is the northerly component, and w is upward component, then equation (4) can be written as

$$\begin{pmatrix} v \\ -u \\ -w \end{pmatrix} = (R)(P)(Y) \begin{pmatrix} u' \\ v' \\ w' \end{pmatrix} \quad (5)$$

The Euler angles (roll, pitch, and yaw) in the 1 Hz data files are defined such that roll is a right-handed rotation about the $+z'$ axis, pitch is a right-handed rotation about $+y'$ axis, and yaw is a right-handed rotation about the $-x'$ axis (or left-handed rotation about the $+x'$ axis). These matrices are given by

$$(R) = \begin{pmatrix} \cos \varepsilon_r & \sin \varepsilon_r & 0 \\ -\sin \varepsilon_r & \cos \varepsilon_r & 0 \\ 0 & 0 & 1 \end{pmatrix}, \quad (6)$$

$$(P) = \begin{pmatrix} \cos \varepsilon_p & 0 & \sin \varepsilon_p \\ 0 & 1 & 0 \\ -\sin \varepsilon_p & 0 & \cos \varepsilon_p \end{pmatrix}, \quad (7)$$

and

$$(Y) = \begin{pmatrix} 1 & 0 & 0 \\ 0 & \cos \varepsilon_y & -\sin \varepsilon_y \\ 0 & \sin \varepsilon_y & \cos \varepsilon_y \end{pmatrix}, \quad (8)$$

where ε_r , ε_p , and ε_y are the Euler angles for roll, pitch, and yaw, respectively. The transformation in equation (5) implies that the x' axis points north, the y' axis points west, and the z' axis points down when $\varepsilon_r = \varepsilon_p = \varepsilon_y = 0$.

Figure 5 shows a typical hour-long time series of ε_r , ε_p , and ε_y from the Vindicator III on the Virginia buoy for 10 May, 2015. We note that the angular limits for each of the Euler angles are given by $|\varepsilon_r| \leq 180^\circ$, $|\varepsilon_y| \leq 180^\circ$, and $|\varepsilon_p| \leq 90^\circ$. From Fig 5 we see that the pitch angle, ε_p , tends to fluctuate near its upper limit of 90° , which corresponds to a zenith orientation of the x' axis when $\varepsilon_r = \varepsilon_p = 0$.

Since the pitch angle is constrained to values between $\pm 90^\circ$, the roll and yaw angles are forced to jump by $\pm 180^\circ$ as the x' axis pitches through zenith, a condition commonly referred to as gimbal lock. Although the gimbal lock problem presents an inconvenience since it causes discontinuities in the attitude angles, it does not impact the pointing accuracy of the laser beams.

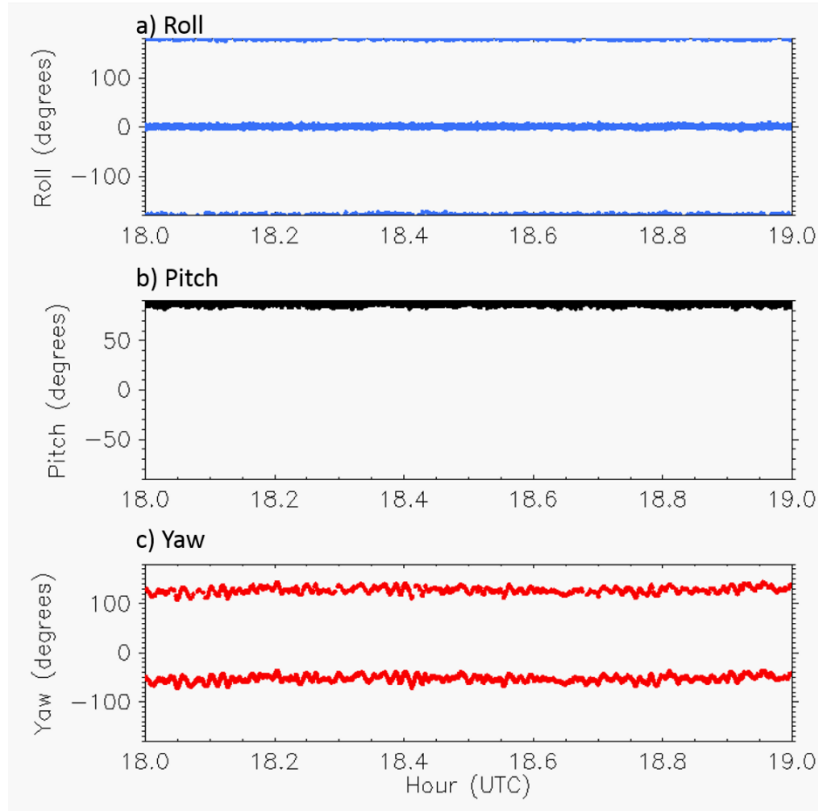


Figure 5. Time series of roll, pitch, and yaw from the Vindicator III AHRS unit on the Virginia buoy between 18:00 to 19:00 UTC on 10 May, 2015. Note the gimbal lock issue.

The final reported values of wind speed, direction, and vertical velocity in the 1 Hz data files are obtained by smoothing the velocity components from equation (5) using a 60-sec running box-car average. This smoothing operation has a significant effect on the reported wind speeds, directions, and vertical velocities. As an example, Figure 6 shows representative time series of wind speed and direction for the smoothed results from the 1 Hz data files (red) and the unsmoothed results (blue) obtained by reprocessing the 1 Hz radial velocity data using Equation (5).

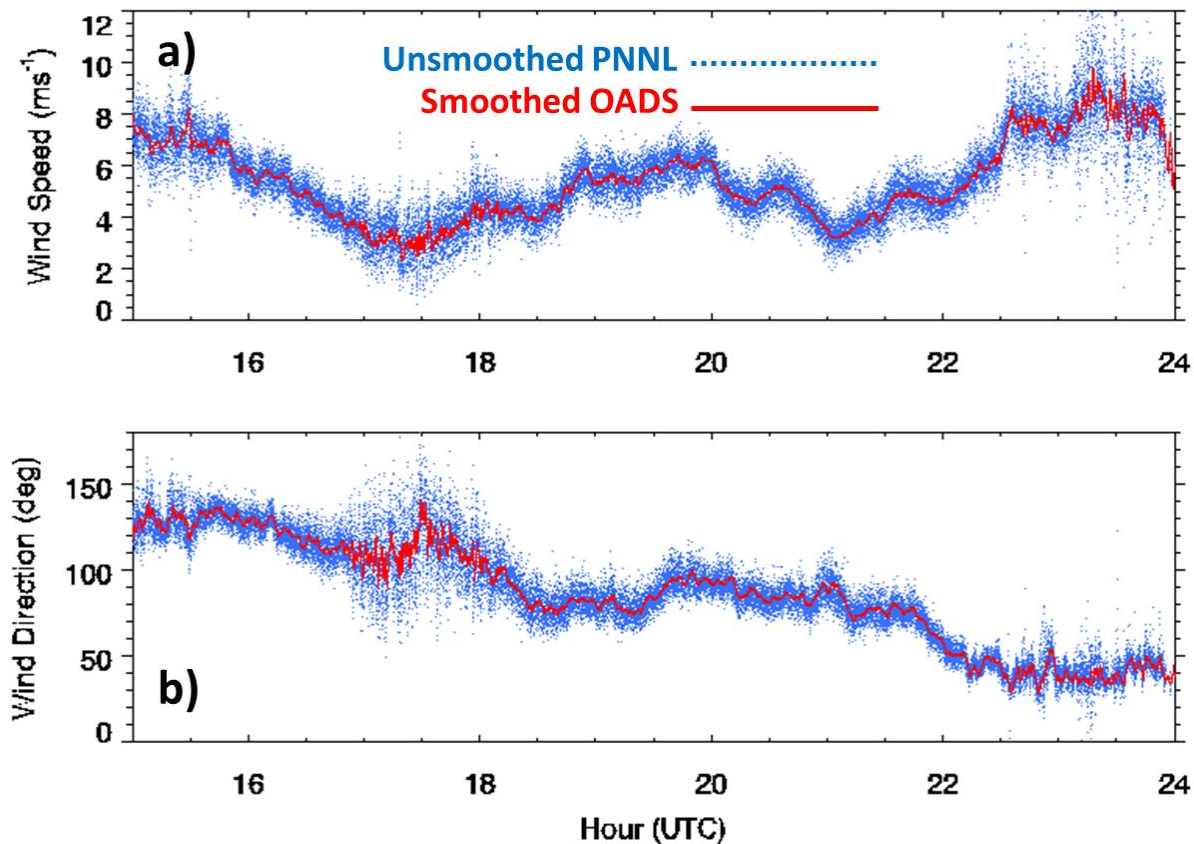


Figure 6. Representative time series of 1 Hz a) wind speed and b) wind direction of the smoothed OADS (red) and unsmoothed (blue) retrievals. This example was taken from 4 June, 2015.

4.0 PNNL Wind Retrieval and Results

The PNNL wind retrieval and attitude correction approach is essentially identical to the OADS approach as described in the previous section except that the final smoothing operation is not performed. Instead, 10-minute averages are computed from the unsmoothed 1 Hz output of equations (3) and (5) by filtering out estimates that fall below a predefined signal-strength threshold (S_T). Additionally, within each 10-minute averaging interval only those samples with wind speeds that fall between the 5th and 95th percentiles are included in the average. This helps to reduce the effect of outliers.

Biases in the retrieved wind speeds can be caused by biases in the Doppler shift estimates (and corresponding radial velocities). In the weak signal regime, these biases can arise when the Doppler noise spectrum exhibits a systematic variation across the passband (Frehlich et al. 1997). Most systems are designed to perform periodic noise measurements and to use those measurements to correct for the variation in the noise floor (Grund et al. 2001, Pearson et al. 2009). However, in practice the correction is often imperfect so there remains some small systematic variation. Since Doppler shift estimators operate by locating the global maximum in the Doppler spectrum (Rye and Hardesty 1997), the probability of picking out the peak in the noise floor (instead of the signal peak) increases as the signal gets weaker.

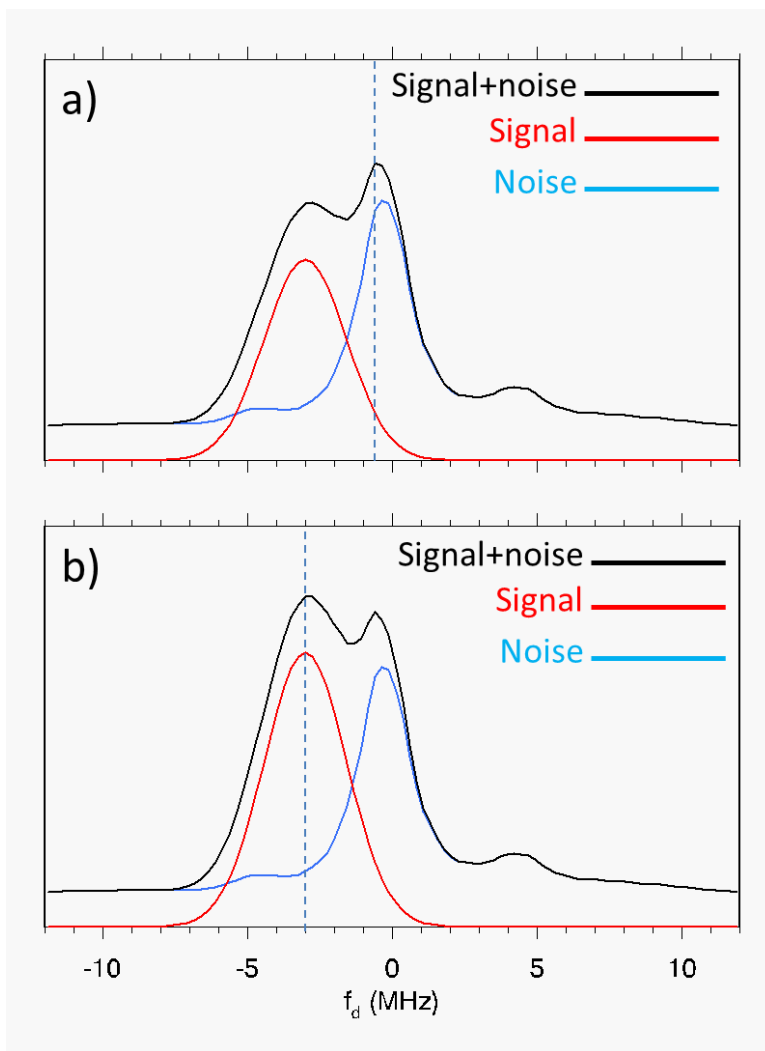


Figure 7. Doppler frequency shift estimation in the weak signal regime. The blue curves in both plots are noise spectra from a Halo Photonics StreamLine Doppler lidar operated by the DOE ARM facility, and the red curves represent idealized signal spectra. In (a) the global maximum in the total spectrum (signal+noise) is close to the peak in the noise spectrum, resulting in a false detection. In (b) the global maximum in the total spectrum coincides with the signal peak, resulting in a good detection.

Figure 7 illustrates the difficulty associated with detection in the weak signal regime. The blue curves represent real noise spectra obtained from a Halo Photonics StreamLine Doppler lidar operated by the DOE ARM facility (sgpd1C1, 16 June 2014). The red curves represent idealized (Gaussian) signal spectra with center frequencies located at 3 MHz. In Figure 7b the signal is just strong enough such that the global maximum in the total spectrum (black, signal+noise) coincides with the signal peak, resulting in a good detection. In Figure 7a the signal is slightly weaker such that the global maximum in the total spectrum occurs close to the noise peak, resulting in a false detection. In this case, the influence of the noise floor causes the Doppler frequency shift estimates (and corresponding radial velocities) to be biased toward zero, and this, in turn, causes the wind speeds computed from equations (3) and (5) to be slow biased.

Biases in the 10-minute average winds can be minimized by rejecting false detections in the 1-sec data through the application of a signal strength threshold (S_T). The problem then becomes one of objectively

determining an appropriate S_T . If a collocated calibrated reference wind measurement were available, the optimal S_T could be determined by examining the behavior of the mean difference between the lidar and the reference as a function of the S_T . We would expect the mean difference to asymptotically approach zero as the S_T is increased.

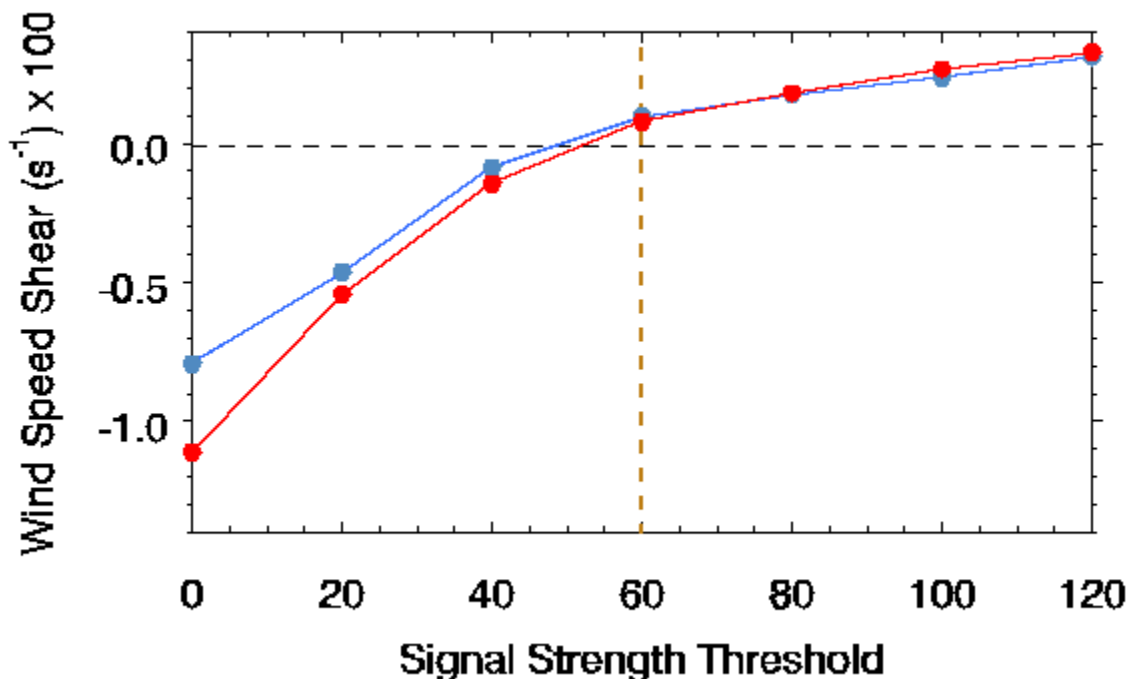


Figure 8. Mean wind speed shear between third and fifth gates (blue) and third and sixth range gates (red) as a function of signal strength threshold, S_T . The averages were computed over the period from 13 December, 2014 to 8 March, 2016.

For this study, we have no reference measurement to compare against. Instead, we examine the effect that the S_T has on the mean wind speed shear in the upper two range gates (i.e., range gates 5 and 6). The idea here is that the mean shear will asymptotically approach a limiting value as the S_T increases due to a reduction in the slow biases in the upper gates. To investigate we generated multiple data sets of 10-minute averages from the reprocessed 1 Hz data using S_T values ranging from 0 to 120. Figure 8 shows plots of the mean wind speed shear between the fifth and third gates (red) and the sixth and third range gates (blue). The averages were computed over the period from 13 December, 2014 through 8 March, 2016. Both curves exhibit sharp increases in the shear as the S_T is increased from 0 to about 60. Above an S_T of 60, the curves increase more gradually, in an approximately linear fashion. We speculate that the increase in shear for $S_T > 60$ is due to a conditional sampling effect in which higher thresholds tend to favor cases with higher wind speeds and therefore stronger shear. The higher wind speeds cause more sea-spray, and therefore more salt particles to be lofted into the lower atmosphere, resulting in stronger lidar backscatter.

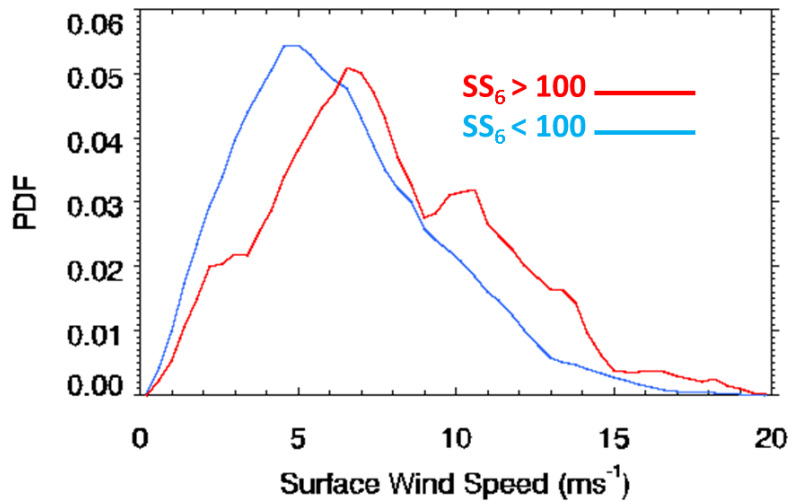


Figure 9. Distributions of the surface wind speed for $S_6 > 100$ (red) and $S_6 < 100$ (blue). These curves were computed using data spanning the period from 13 December, 2014 through 9 March, 2016.

Figure 9 displays surface wind speed distributions based on the signal strength of the highest lidar range gate, S_6 . The red (blue) curve shows the distribution of surface wind speed when the signal strength of the sixth lidar range gate is greater than (less than) 100. We note that the mean surface wind speed is 6.6 ms^{-1} for $S_6 < 100$, and 7.8 ms^{-1} for $S_6 > 100$. It is clear from Figure 9 that higher surface wind speeds tend to be associated with higher signal strengths. This is consistent with the notion that stronger winds generate more sea spray, which increases the concentration of salt particles in the lower atmosphere.

The signal strength threshold, S_T , should be high enough to remove most of the biased 1 Hz data, while small enough to allow reasonable data recovery. For this study, we decided to go with an S_T of 60 based on the results shown in Figure 8. Figure 10 shows the diurnal and seasonal variation in the data recovery rates for the third and sixth range gates when $S_T = 60$. For comparison, the median signal strength is also shown. We note that the data recovery tends to track variations in the signal strength. Figure 10b shows that the signal strength is lowest during the winter and highest in the summer. Figure 10a shows that the signal strength is lowest during the nighttime and highest during the daytime. These seasonal and diurnal variations are consistent with long-term lidar observations in the mid-latitudes over land (Matthias and Bosenberg 2002, Turner et al. 2001), and reflect the natural variability in aerosol backscatter.

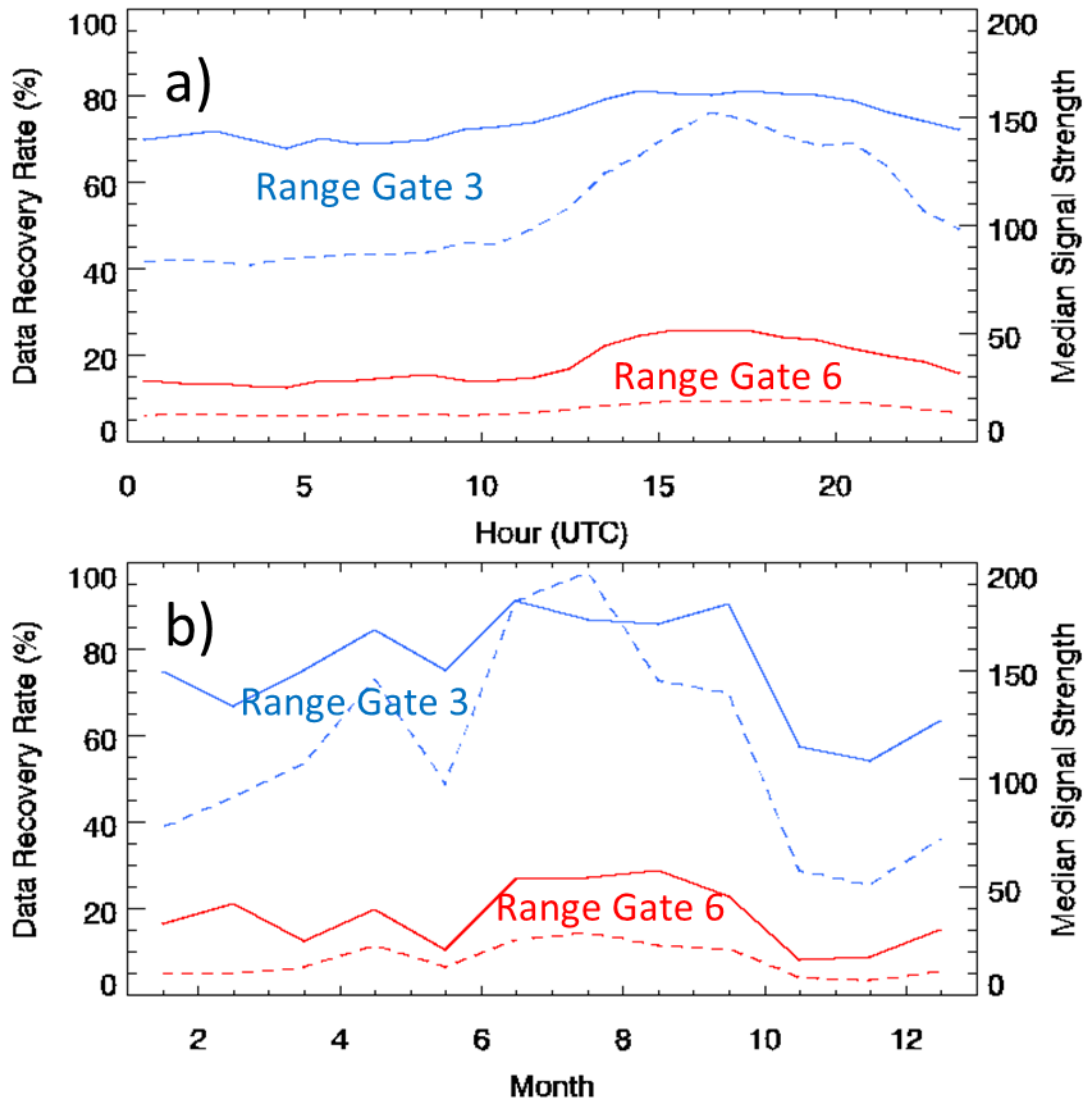


Figure 10. a) Diurnal and b) seasonal data recovery (solid) and signal strength (dashed) for $S_T=60$. The highest and lowest data recovery rates occur for the third (blue) and sixth (red) range gates, respectively.

Figure 11 illustrates the effect of the signal strength threshold on the mean wind speed and wind shear profiles using $S_T=0$ and $S_T=60$. These results were obtained by averaging profiles for time periods between 15 and 20 UTC on all days between 1 June and 30 September, 2015. As such, the profiles are representative of conditions during the daytime in the summer months. Figure 11a shows that the wind speeds for $S_T=60$ are larger than for $S_T=0$. This is due to the fact that higher thresholds tend to filter out lower-wind-speed cases, as discussed previously. The overall effect of the signal strength threshold is to decrease the magnitude of the shear, both above and below the maxima in the profiles, as illustrated in Figure 11b. The shear profile is most affected where the signal strength is weakest, as expected.

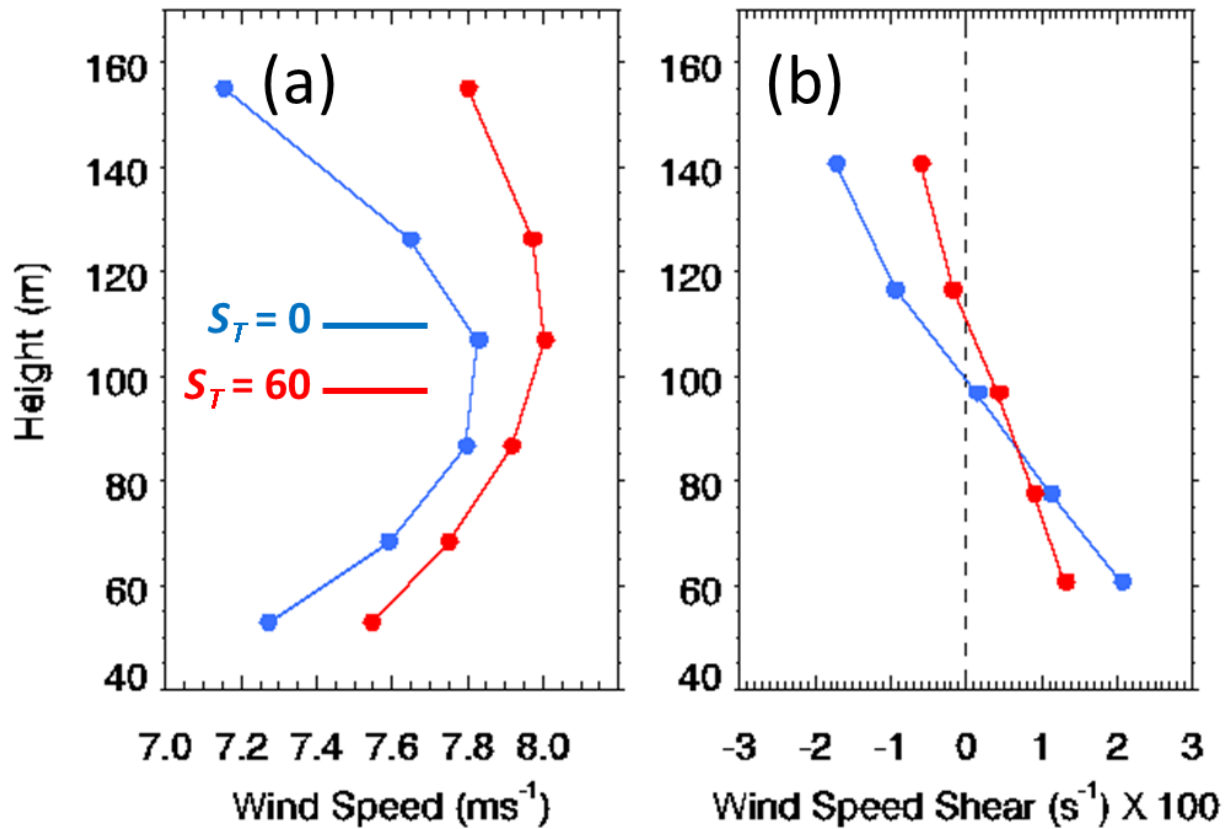


Figure 11. Mean daytime wind speed (a) and shear (b) profiles for the period from 1 June through 30 September, 2015 using $S_T=0$ (blue) and $S_T=60$ (red).

One other issue to mention here concerns the height of the reported wind speed, direction, and vertical velocity measurements. Since the attitude of the lidar is continually changing, it is inappropriate to equate the range coordinate to the measurement height. In general, for a given range gate, the height coordinate for each beam is different, and these heights change in time as the buoy is subjected to roll, pitch, and yaw motions. In the PNNL approach, the height coordinates of the 1 Hz measurements are computed from an average of the three beams. Similarly, the height coordinates reported in the 10-minute average data files are computed by averaging the 1 Hz height coordinates of those samples with signal strengths greater than the prescribe threshold. As a result, the height arrays in the PNNL results depend on time and are therefore stored as two-dimensional arrays.

In practice, the effect of the buoy motion on the measurement height is generally quite small. Figure 12 shows a time series of the 10-minute-averaged measurement heights for the month of June 2015. Also, Table 2 lists the mean measurement heights and corresponding standard deviations for each range gate for the period from 13 December, 2014 to 8 March, 2016. The variability in the measurement height for any given range gate is very small, as indicated in both Figure 12 and Table 2. Thus, it is sufficient to simply use the mean measurement height for each range gate when analyzing the wind data from the lidar.

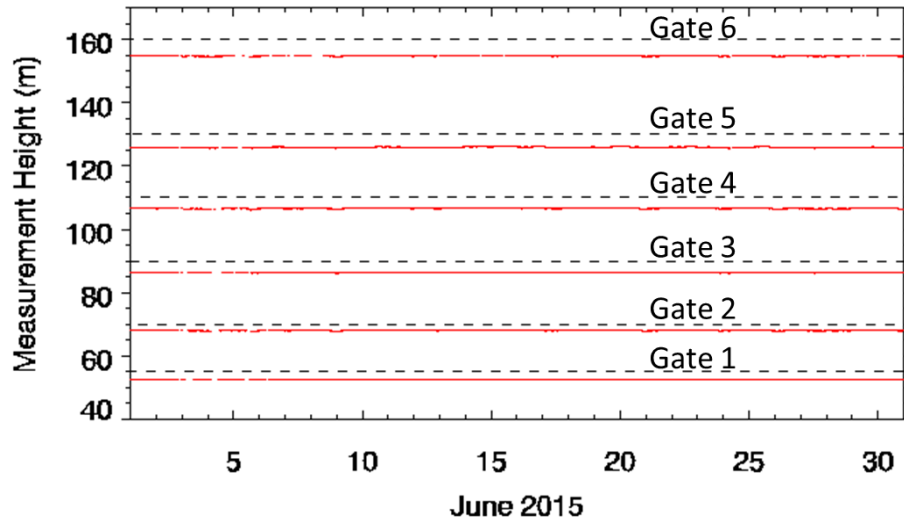


Figure 12. 10-minute-averaged lidar measurement heights (red) for the month of June 2015. The black dashed lines indicate the lidar-to-range-gate distance.

Table 2. Mean measurement heights (third column) and corresponding standard deviations (fourth column) for the period from 13 December, 2014 to 8 March, 2016.

Gate #	Range (m)	Mean Height (m)	Standard Deviation (m)
1	55	53.0	0.07
2	70	68.4	0.09
3	90	86.7	0.12
4	110	107.0	0.14
5	130	126.2	0.17
6	160	155.1	0.21

5.0 Summary

Mean wind profiles obtained from the Vindicator III lidar during the Virginia deployment of the DOE WindSentinel buoy consistently show wind speed maxima at about the 90 m level, and unexpectedly high negative shears above that level. The apparent maximum in the wind speed profile is believed to be the result of slow biases in the upper range gates due to the influence of systematic noise when the backscatter signal is weak. In this study, we attempt to address this issue by first reexamining the way in which the 1 Hz OADS winds were computed, and then by applying more aggressive filtering of the 1 Hz data based on the return signal strength.

It was confirmed that the 1 Hz OADS wind retrievals are based on the application of equations (3) and equation (5). As a final processing step, the wind speeds, wind directions, and vertical velocities are subjected to a smoothing operation in which a box-car average is applied to the preceding 60 seconds of measurements. This low-pass filtering operation has a minimal effect on the 10-minute averages, but may have a larger impact on shorter-term averages due to the phase shift that it introduces. The PNNL approach is also based on the application of equations (3) and (5); however, the resulting 1 Hz data are

not smoothed. Instead, 10-minute averages are computed from the unsmoothed 1 Hz output of equations (3) and (5) by filtering out estimates that fall below a predefined signal-strength threshold, S_T . Additionally, within each 10-minute averaging interval, only those samples with wind speeds that fall between the fifth and 95th percentiles are included in the average in order to reduce the effect of outliers.

The signal strength threshold, S_T , was determined by examining the effect that it has on the wind shear in the upper two range gates. We found that the shear increased sharply as S_T is increased from 0 to about 60. For $S_T > 60$, the shear increased more gradually. Based on these results, we selected $S_T = 60$ for processing the 10-minute-averaged winds.

The overall effect of the signal strength threshold is to decrease the magnitude of the shear, both above and below the apparent maxima in the wind speed profile. The effect is most pronounced in the highest range gates where the return signal strength is generally weakest. Another effect of the signal strength threshold is a reduction in the data recovery rate. For $S_T = 60$, the annually averaged data recovery rate was about 75% for the best case (range gate 3), and about 15 to 20% for the worst case (range gate 6). Data recovery rates are higher during the warm season and during daytime periods. We also found that lower-wind-speed cases tend to be filtered out as S_T is increased. It is believed that higher winds cause more sea spray, which results in stronger lidar return signals.

6.0 References

Frehlich R, SM Hannon, and SW Henderson. 1997. "Coherent Doppler lidar measurements of winds in the weak signal regime." *Applied Optics* 36(15): 3491-3499, [doi:10.1364/AO.36.003491](https://doi.org/10.1364/AO.36.003491).

Grund, CJ, RM Banta, JL George, JN Howell, MJ Post, RA Richter, and AM Weickmann. 2001. "High-resolution Doppler lidar for boundary layer and cloud research." *Journal of Atmospheric and Oceanic Technology* 2001; 18: 376-393, [doi:10.1175/1520-0426\(2001\)018<0376:HRDLFB>2.0.CO;2](https://doi.org/10.1175/1520-0426(2001)018<0376:HRDLFB>2.0.CO;2).

Lundquist JK, JM Wilczak, R Ashton, L Bianco, WA Brewer, A Choukulkar, A Cliftn Mithu Debnath, R Delgado K Friedrich, S Gunter, A Hamidi, GV Iungo, A Kaushik, B Kosovic P Langan, A Lass E Lavin, JC-Y Lee, KL McCaffrey, RK Newsom, DC Noone, SP Oncley, PT Quelet, SP Sandberg, JL Schroeder, WJ Shaw, L Sparling, C St. Martin, A St. Pe, E Strobach, K Tay, BJ Vanderwende, A Weickmann, D Wolfe, and R Worsnop. 2016. "Assessing state-of-the-art capabilities for probing the atmospheric boundary layer: the XPIA field campaign." *Bulletin of the American Meteorological Society*, accepted, [doi:10.1175/BAMS-D-15-00151.1](https://doi.org/10.1175/BAMS-D-15-00151.1).

Matthias V and J Bosenberg. 2002. "Aerosol climatology for the planetary boundary layer derived from regular lidar measurements." *Atmospheric Research* 63(3-4): 221-245, [doi:10.1016/S0169-8095\(02\)00043-1](https://doi.org/10.1016/S0169-8095(02)00043-1).

Newsom RK, S Matzner, M Pekour, WJ Shaw, JA Ward, G Matzat, A Duerr, and JW Cline. 2015. "New DOE lidar buoys: Evaluation of lidar wind profiles obtained during initial offshore performance tests." Presentation at the American Meteorological Society annual meeting, Phoenix, Arizona, <https://ams.confex.com/ams/95Annual/webprogram/Paper267918.html>

Pearson G, F Davies, and C Collier. 2009. "An analysis of the performance of the UFAM pulsed Doppler lidar for observing the boundary layer." *Journal of Atmospheric and Oceanic Technology* 26: 240-250, [doi:10.1175/2008JTECHA1128.1](https://doi.org/10.1175/2008JTECHA1128.1).

Rye, BJ and RM Hardesty, 1997. "Detection techniques for validating Doppler estimates in heterodyne lidar." *Applied Optics* 36(9): 1940-1951, [doi:10.1364/AO.36.001940](https://doi.org/10.1364/AO.36.001940).

Turner DD, RA Ferrare, and LA Brasseur. 2001. "Average Aerosol Extinction and Water Vapor Profiles over the Southern Great Plains." *Geophysical Research Letters* 28(23): 4441-4444, [doi:10.1029/2001GLO13691](https://doi.org/10.1029/2001GLO13691).

Appendix A

Vindicator versus Tower Comparison during XPIA

During the XPIA field campaign in April and May of 2015, several profiling Doppler lidars systems were deployed approximately 130 m south of the BAO tower. This included two Vindicator III lidars on loan from AXYS Technologies that were identical in design to the lidar on board the Virginia WindSentinel buoy. One Vindicator was deployed on the ground and one Vindicator was mounted nearby on a motion table. Here we present a comparison between the stationary ground-based Vindicator (S/N 3013) and the BAO tower measurements.

During XPIA, the BAO tower was instrumented with sonic anemometers at 50, 100, 150, 200, 250 and 300 m, and the Vindicator lidars were configured with range gate centers at 55, 60, 80, 100, 120 and 150 m. Each BAO tower level had two sonic anemometers, one mounted on a southeast boom (at a heading angle of 154°) and one mounted on a northwest boom (at a heading angle 334°). To minimize tower wake effects, only data from the upwind side of the tower were used in the comparisons. The sonic anemometer data were corrected for tilt and screened for poor-quality measurements (Lundquist et al. 2016). The 20 Hz sonic data and 1 Hz Vindicator data were averaged down to 10 minutes using scalar averaging for the wind speeds and vector averaging for the wind directions. Vindicator measurements were corrected for the local magnetic declination angle (approximately $+8.5^\circ$ at the BAO on April 1, 2015). To facilitate a comparison between the tower and the Vindicators, the tower wind measurements were linearly interpolated to the range gate center heights of the Vindicators.

Comparisons are performed with and without a signal strength threshold applied to the Vindicator measurements. Figures A1 and A2 show scatter plots of the sonic wind speeds versus the Vindicator wind speeds for all range gates. Figure A1 shows the result with no signal strength threshold, and Figure A2 shows the result using a signal strength threshold of 50. Similarly, Tables 1 and 2 list wind speed biases, difference standard deviations, correlation coefficients, linear regressions, and data availabilities. Table 1 shows the results with no signal strength threshold, and Table 2A shows the results with a threshold of 50.

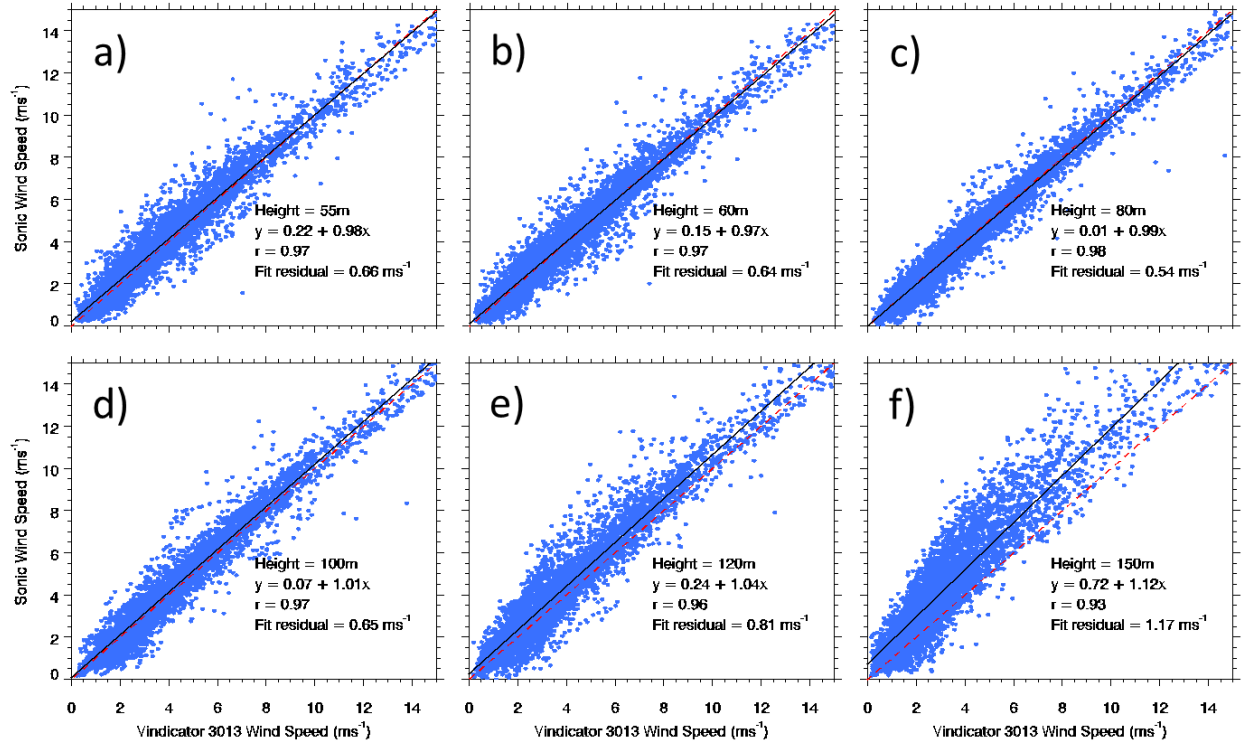


Figure A.1 Correlation diagrams showing sonic wind speeds versus Vindicator_3013 wind speeds using $S_T=0$ at a) 55 m, b) 60 m, c) 80 m, d) 100 m, e) 120 m, and f) 150 m AGL.

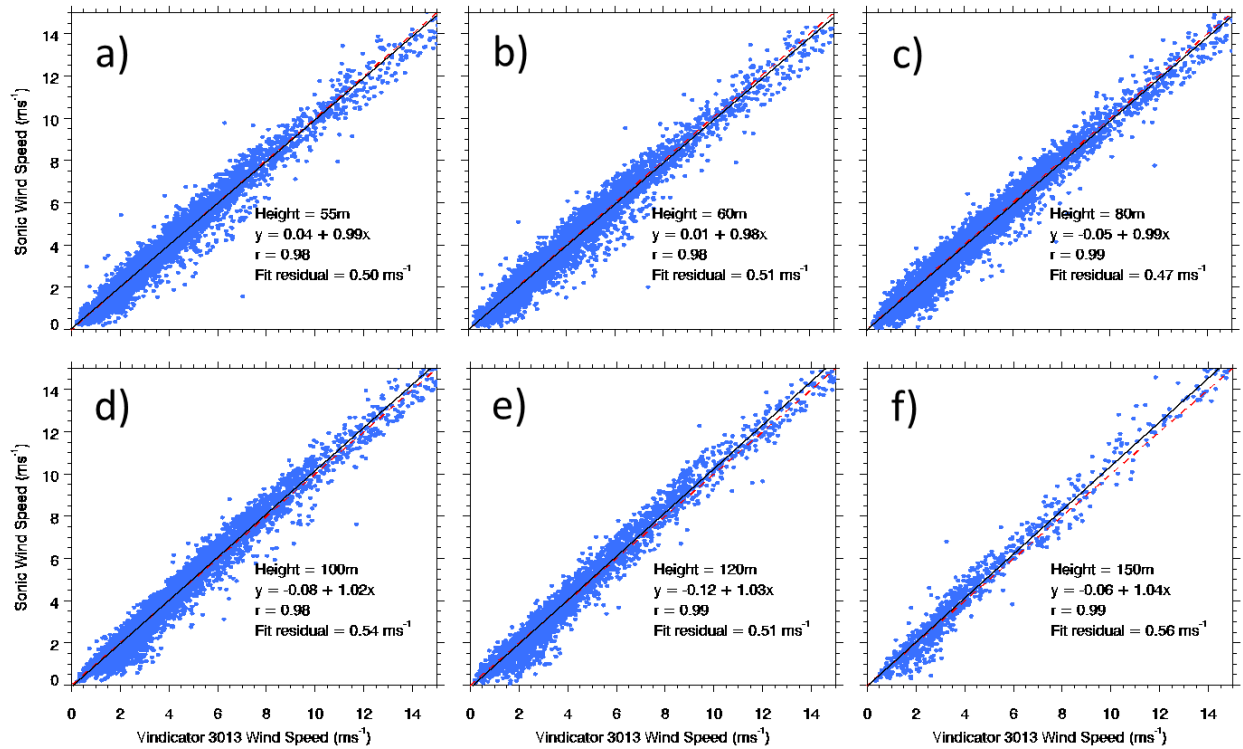


Figure A.2. Correlation diagrams showing sonic wind speeds versus Vindicator_3013 wind speeds using $S_T=50$ at a) 55 m, b) 60 m, c) 80 m, d) 100 m, e) 120 m, and f) 150 m AGL.

In Tables 1A and 2A the wind speed bias is defined as

$$\Delta_{wspd} = \overline{U_{lidar} - U_{sonic}} \quad (A1)$$

where U_{lidar} is the Vindicator wind speed, and U_{sonic} is the sonic wind speed. The relative wind speed bias is given by

$$\Delta_{wspd}^{rel} = \overline{\Delta_{wspd} / U_{sonic}} \quad (A2)$$

The standard deviation of the wind speed bias is denoted as σ_{wspd} , and the Pearson linear correlation coefficient is denoted r_{wspd} . The wind direction difference is computed using

$$\Delta_{wdir} = \tan^{-1} \left(\frac{\cos \phi_{sonic} \sin \phi_{lidar} - \sin \phi_{sonic} \cos \phi_{lidar}}{\sin \phi_{sonic} \sin \phi_{lidar} + \cos \phi_{sonic} \cos \phi_{lidar}} \right)$$

where ϕ_{lidar} and ϕ_{sonic} are the vector wind directions for the lidar and the sonic anemometers, respectively.

The standard deviation of the wind direction difference is denoted as σ_{wdir} . The overbars in the above definitions imply temporal averaging. Positive (negative) wind direction biases imply that the Vindicator winds are rotated clockwise (counter-clockwise) relative to the sonic winds. For the wind direction statistics, we used only wind speeds greater than 1 ms^{-1} , as determined from the sonic anemometers.

Table A.1. Comparison between the BAO tower and the Vindicator lidar (S/N 3013) during XPIA (from 8 April to 29 May, 2015). No signal strength threshold was applied to the Vindicator measurements.

Height (m)	Wind Speed						Wind Direction		Data Recovery (%)
	Δ_{wspd} (ms^{-1})	Δ_{wspd}^{rel} (%)	σ_{wspd} (ms^{-1})	Regression		r_{wspd}	Δ_{wdir} (deg)	σ_{wdir} (deg)	
			offset (ms^{-1})	Slope					
55	-0.143	-3.44	0.663	0.222	0.980	0.968	-21.294	14.274	83
60	-0.044	-1.05	0.645	0.149	0.975	0.971	-21.231	13.976	83
80	0.037	0.84	0.545	0.015	0.988	0.981	-21.011	13.431	83
100	-0.126	-2.78	0.656	0.066	1.014	0.975	-21.043	14.514	82
120	-0.394	-8.60	0.821	0.238	1.037	0.963	-22.467	14.797	82
150	-1.135	-24.37	1.207	0.723	1.117	0.930	-24.008	17.030	81

Table A.2. Comparison between the BAO tower and the Vindicator lidar (S/N 3013) during XPIA (from 8 April to 29 May 2015). A signal strength threshold of 50 was applied to the Vindicator measurements.

Height (m)	Wind Speed						Wind Direction		Data Recovery (%)
	Δ_{wspd} (ms^{-1})	Δ_{wspd}^{rel} (%)	σ_{wspd} (ms^{-1})	Regression		r_{wspd}	Δ_{wdir} (deg)	σ_{wdir} (deg)	
			offset (ms^{-1})	Slope					
55	0.013	0.31	0.501	0.039	0.987	0.983	-21.310	14.903	65
60	0.059	1.41	0.515	0.009	0.984	0.982	-21.272	14.031	71
80	0.088	2.03	0.471	-0.053	0.992	0.986	-21.062	13.601	77
100	-0.019	-0.42	0.542	-0.080	1.022	0.984	-21.171	14.966	70
120	-0.037	-0.82	0.524	-0.117	1.034	0.988	-22.475	16.011	46
150	-0.141	-2.87	0.586	-0.056	1.041	0.990	-24.887	17.002	14

It is clear from Tables 1A and 2A that signal strength threshold is effective at reducing the overall wind speed differences between the tower and the lidar. However, a negative consequence of the filtering is a significant reduction in the data recovery rates. We also note that in this case the wind directions exhibit large biases (~ -21 to -24°). This occurred because the magnetic sensor (part of the AHRS) was not properly calibrated prior to the XPIA deployment.

Appendix B

Data File Description and Format for the 1 Hz OADS Vindicator III Data

The Vindicator III lidar outputs data files containing the raw radial velocities, signal strengths, sensor roll, pitch and yaw, wind speed and direction, and various ancillary fields (e.g. internal temperature, pressure and humidity) at one-second time resolution. These raw files have been translated by PNNL from their native hexadecimal format into daily NetCDF

(http://www.unidata.ucar.edu/software/netcdf/docs/user_guide.html) files. The contents of these NetCDF files are described below.

```
netcdf va1buoyvindicatorB1.b1.20160301.000000 {
```

```
dimensions:
```

```
    time = UNLIMITED ; // (86073 currently)
```

```
    range_gate = 6 ;
```

```
variables:
```

```
    int base_time ;
```

```
        base_time:string = "2016-03-01 00:00:00 0:00" ;
```

```

    base_time:long_name = "Base time in Epoch" ;
    base_time:units = "seconds since 1970-1-1 0:00:00 0:00" ;
double time_offset(time) ;
    time_offset:long_name = "Time offset from base_time" ;
    time_offset:units = "seconds since 2016-03-01 00:00:00 0:00" ;
double time(time) ;
    time:long_name = "Time offset from midnight" ;
    time:units = "seconds since 2016-03-01 00:00:00 0:00" ;
    time:calendar = "gregorian" ;
    time:standard_name = "time" ;
float range(time, range_gate) ;
    range:long_name = "Range from vindicator to center of the range gate" ;
    range:units = "m" ;
float pitch(time) ;
    pitch:long_name = "Vindicator pitch angle" ;
    pitch:units = "degrees" ;
float roll(time) ;
    roll:long_name = "Vindicator roll angle" ;
    roll:units = "degrees" ;
float yaw(time) ;
    yaw:long_name = "Vindicator yaw angle from magnetic north" ;
    yaw:units = "degrees" ;
float pitch_rate(time) ;
    pitch_rate:long_name = "Pitch angular velocity" ;
    pitch_rate:units = "degrees/s" ;
float roll_rate(time) ;
    roll_rate:long_name = "Roll angular velocity" ;
    roll_rate:units = "degrees/s" ;
float yaw_rate(time) ;
    yaw_rate:long_name = "Yaw angular velocity" ;
    yaw_rate:units = "degrees/s" ;
short qc_wind(time) ;
    qc_wind:long_name = "QC for each range gate" ;
    qc_wind:units = "unitless" ;
short laser_status(time) ;
    laser_status:long_name = "Status of laser" ;
    laser_status:units = "unitless" ;
float sig_laser_0(time, range_gate) ;
    sig_laser_0:long_name = "Return signal strength along beam 0, signal amplitude" ;
    sig_laser_0:units = "a.u." ;
float sig_laser_1(time, range_gate) ;
    sig_laser_1:long_name = "Return signal strength along beam 1, signal amplitude" ;
    sig_laser_1:units = "a.u." ;
float sig_laser_2(time, range_gate) ;
    sig_laser_2:long_name = "Return signal strength along beam 2, signal amplitude" ;
    sig_laser_2:units = "a.u." ;
float ur_laser_0(time, range_gate) ;
    ur_laser_0:long_name = "Radial velocity along beam 0" ;
    ur_laser_0:units = "m/s" ;
    ur_laser_0:comment = "Positive values indicate motion away from the lidar" ;
float ur_laser_1(time, range_gate) ;
    ur_laser_1:long_name = "Radial velocity along beam 1" ;
    ur_laser_1:units = "m/s" ;

```

```

        ur_laser_1:comment = "Positive values indicate motion away from the lidar" ;
float ur_laser_2(time, range_gate) ;
        ur_laser_2:long_name = "Radial velocity along beam 2" ;
        ur_laser_2:units = "m/s" ;
        ur_laser_2:comment = "Positive values indicate motion away from the lidar" ;
float horizontal_wspd(time, range_gate) ;
        horizontal_wspd:long_name = "Motion corrected wind speed" ;
        horizontal_wspd:units = "m/s" ;
float horizontal_wdir(time, range_gate) ;
        horizontal_wdir:long_name = "Motion corrected wind direction relative to magnetic north" ;
        horizontal_wdir:units = "degrees" ;
        horizontal_wdir:comment = "0 degree means wind from magnetic North (compass mode)" ;
float vertical_velocity(time, range_gate) ;
        vertical_velocity:long_name = "Vertical velocity" ;
        vertical_velocity:units = "m/s" ;
float relative_humidity(time) ;
        relative_humidity:long_name = "Internal instrument relative humidity" ;
        relative_humidity:units = "percent" ;
float air_pressure(time) ;
        air_pressure:long_name = "Internal instrument air pressure" ;
        air_pressure:units = "kPa" ;
float temperature_1(time) ;
        temperature_1:long_name = "Internal instrument temperature from sensor 1" ;
        temperature_1:units = "degrees C" ;
float temperature_2(time) ;
        temperature_2:long_name = "Internal instrument temperature from sensor 2" ;
        temperature_2:units = "degrees C" ;
float temperature_3(time) ;
        temperature_3:long_name = "Internal instrument temperature from sensor 3" ;
        temperature_3:units = "degrees C" ;
float temperature_4(time) ;
        temperature_4:long_name = "Internal instrument temperature from sensor 4" ;
        temperature_4:units = "degrees C" ;
float latitude(time) ;
        latitude:long_name = "Latitude" ;
        latitude:units = "degrees" ;
float longitude(time) ;
        longitude:long_name = "Longitude" ;
        longitude:units = "degrees" ;

// global attributes:
        :data_description = "1-sec Vindicator III data from DOE buoy 6NB00120 during the Virginia
deployment" ;
        :altitude_air_temperature_humidity_sensor = "3 m ASL" ;
        :altitude_surface_wind_speed_sensor = "4 m ASL" ;
        :altitude_surface_wind_direction_sensor = "4 m ASL" ;
        :altitude_lidar = "3 m ASL" ;
        :altitude_solar_radiation_sensor = "4 m ASL" ;
        :altitude_sea_water_sensor = "0 m ASL" ;
        :altitude_CTD_sensor = "0 m ASL" ;
        :altitude_ADCP_sensor = "-0.65 m ASL" ;
        :serial_number = "3010 " ;
}

```




Pacific Northwest
NATIONAL LABORATORY

*Proudly Operated by **Battelle** Since 1965*

902 Battelle Boulevard
P.O. Box 999
Richland, WA 99352
1-888-375-PNNL (7665)

U.S. DEPARTMENT OF
ENERGY

www.pnnl.gov